Propagative Landau States and Fermi Level Pinning in Carbon Nanotubes

Sébastien Nanot,[1] Rémi Avriller,[2] Walter Escoffier,[1] Jean-Marc Broto,[1] Stephan Roche,[3,4] and Bertrand Raquet[1]

[1]*Laboratoire National des Champs Magnétiques Intenses, INSA UPS CNRS, UPR 3228, Université de Toulouse, 143 avenue de rangueil, 31400 Toulouse, France*

[2]*Departamento de Física Teórica de la Materia Condensada C-V, Facultad de Ciencias, Universidad Autónoma de Madrid, E-28049 Madrid, Spain*

[3]*CIN2(CSIC-ICN), Campus UAB, E-08193 Barcelona, Spain*

[4]*Commissariat à l'Energie Atomique, INAC, SP2M, L_{sim}, 17 avenue des Martyrs, Grenoble, France*

(Received 8 July 2009; published 15 December 2009)

We present strong evidence of Landau states formation in multiwalled carbon nanotubes with metallic or semiconducting outer shells, under magnetic fields as high as 60 T. Magnetoconductance data are found to converge to a gate-independent value for semiconducting shells, whereas for metallic shells, the Landau states introduce a strong reintroduction of backscattering and Fermi level pinning close to the charge neutrality point. Electronic band structure and transport calculations provide a consistent interpretation of the experimental data.

DOI: 10.1103/PhysRevLett.103.256801 PACS numbers: 73.63.Fg, 71.70.Di

Carbon nanotubes (CNT), isolated graphene sheets, and graphene nanoribbons (GNR) have revealed remarkable electronic properties [1]. The massless dispersion bands at the charge neutrality point (CNP) drive spectacular phenomena such as anomalously low backscattering and the related long mean free path in metallic nanotubes [2], or the huge charge carrier mobility in graphene layers [3]. CNT and GNR also have a large magnetic field dependence of their 1D subbands in common. In graphene, the high magnetic field behavior of Dirac fermions has been shown to induce an half-integer quantum hall effect [4]. In single and multiwalled carbon nanotubes (MWCNT), while the Aharonov-Bohm phenomena were investigated in-depth for axial magnetic fields [5], the exploration of Landau states in the presence of high transverse magnetic fields has been facing overwhelming technical challenges. On the theoretical side, a drastic change of the 1D dispersion bands has been predicted once the cyclotron radius equals the tube radius [6,7]. The calculations show that the resulting magnetic bands remain dispersive along the tube at large k wave vectors suggesting an inhomogeneous chiral current flowing on the flanks of the tube. At low k vectors, a Landau level spectrum is predicted with the $\sqrt{nB}$ magnetofingerprint of graphene, whatever the CNT chirality [6]. Notwithstanding, an experimental observation of Landau states in CNTs has not yet been achieved and the longitudinal magnetoconductance in the quantum regime remains unexplored.

In this Letter, the contribution of propagative Landau states to magnetotransport in semiconducting and metallic MWCNT shells is experimentally unveiled. For semiconducting shells, the occurrence of a zero-energy Landau state associated with the energy gap closure is found to generate delocalized states close to the Dirac point, despite the presence of disorder and low dimensionality, and irrespective of the electrostatic doping strength. For doped metallic shells, the magnetoconductance also exhibits an upshift of the massive 1D bands in agreement with the formation of Landau states. At the CNP, the reintroduction of the backscattering in the metallic bands clearly evidences the onset of the zero-energy Landau state. Even more spectacular is the pinning of the Fermi level at the CNP in high field. These remarkable features are supported by Landauer-Büttiker simulations of the magnetoconductance of weakly disordered semiconducting and metallic CNTs.

Magnetotransport experiments are carried out on individual MWCNTs [8] deposited on Si/SiO_2 (40 nm) wafer and connected to Pd electrodes. The electrostatic doping is controlled by a back-gate voltage. Following prior experiments on the same structural quality of MWCNTs, rather small distances (L_t) between electrodes, from 150 to 550 nm are chosen to achieve a quasiballistic transport regime. MWCNTs of diameters in the range of 10 to 20 nm are selected to reach the high magnetic field regime under 60 T, corresponding to a dimensionless parameter $\nu = r/l_B$ larger than 1 (r is the tube's radius and $l_B = \sqrt{\hbar/eB}$, the magnetic length) [6]. In the following, we focus on two MWCNTs whose external shells, mainly contributing to the conductance, have been identified, respectively, as behaving as semiconducting and metallic shells, in the light of their Aharonov-Bohm magnetofingerprints [9].

Figure 1 shows the conductance under a 60 T transverse magnetic field performed at 150 K on a 13 ± 2 nm diameter MWCNT with $L_t \approx 550$ nm (AFM). The magnetoconductance (MC) exhibits large variations and a drastic dependence on the gate-induced doping, varying from a strongly positive MC around $V_g \approx 2$ V to a large negative one under high back-gate voltages. Interestingly, the high magnetic field conductances for $\nu \gg 1$ converge to a common value ($\sim 0.7 G_0$), whatever the applied electrostatic potential. The inset shows the zero-field conductance

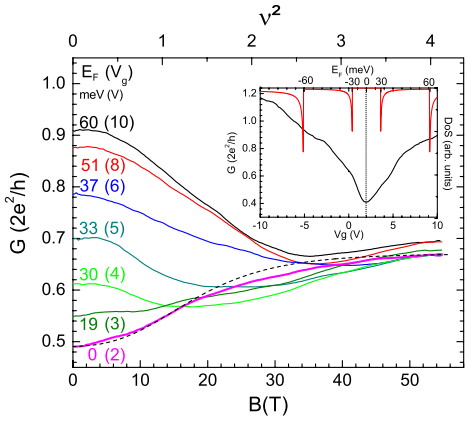

FIG. 1 (color online). Magnetoconductance $G(B)$ at 150 K obtained on a 14 nm MWCNT for selected V_g and the corresponding E_F (see text). The computed conductance close to CNP is shown by a dashed line (see text). Inset: measured conductance versus V_g at zero field. The DOS of a 14 nm semiconducting CNT is also plotted as a function of E_F (upper scale) and V_g (lower scale) deduced from the back-gate coupling.

$G(V_g)$. The symmetrical V-shape curve is ascribed to a semiconducting behavior of the external shell, with a minimum of conductance at $V_g = 2$ V identifying our CNP. A correlated electron-hole Landau level is expected to develop at the neutrality point in both semiconducting and metallic CNTs, inducing a closing of the energy gap in the former case [6]. The magnetic field induced gap suppression is analytically approached by $E_g(\nu) = \Delta_0/I_0(4\nu^2)$, where, I_0 is the zero's order modified Bessel function of first kind and $\Delta_0(\mathrm{eV}) \sim 0.82/d(\mathrm{nm})$, the energy gap at zero field [7]. Assuming thermally activated charge carriers on the external shell at the CNP, the field dependence of the conductance is simply expressed by $\triangle G(B) \propto \exp[-E_g(\nu)/2kT]$. The diameter is fixed to 14 nm, in agreement with the AFM observation. By adjusting the proportionality factor, we consistently reproduce the MC at 2 V (Fig. 1 main frame, dashed line), supporting the field induced gap suppression. The nonlinear relation between the Fermi energy and V_g is defined by $\Delta E_F(\mathrm{eV}) = (C_g/C_{\mathrm{elec}})\mathrm{eV}_g$. The planar capacitance C_g equals 1.2×10^{-1} F $\cdot$ m^{-1} and the electrochemical one, C_{elec}, is deduced from the integrated density of states (DOS). In the inset of Fig. 1, the calculated DOS of a 14 nm semiconducting CNT is plotted as a function of E_F and V_g, assigning the $E_F(V_g)$ correspondence [10].

The MC can now be described as a function of E_F, varying from the CNP to the second diffusive band in the n-doped side. For E_F lying within the energy gap (below 30 meV), the conductance strongly increases with the magnetic field and saturate above $\nu \approx 1.5$. When electrons have filled the second diffusive band, above 50 meV, the conductance is drastically reduced by the magnetic field, but also saturates at similar fields. At intermediate energies, when E_F is close to the first van Hove singularity (vHs) (around 30 meV), the initial decay of a small MC is followed by an upturn at higher fields.

To model the electronic properties of CNTs under magnetic field, a simple π-π coupling Hamiltonian is used with constant first nearest neighbor hopping terms $\gamma_0 = 2.9$ eV. On site energies are either set to zero for disorder-free nanotubes, or taken at random within the interval $[-\frac{W}{2}, \frac{W}{2}]$ to account for some elastic Anderson-type disorder potential. The effect of an external magnetic field is finally included by modulating each hopping matrix element by the so-called Peierls phase [11,12] (see additional information [13]). The transport properties are computed within the framework of Landauer-Büttiker theory [14]. Without disorder, the low-bias conductance at finite temperature is function of the number of available channels and is written as

$$G(E_F, \nu) = \frac{2e^2}{h} \sum_i \int_{E_i(\nu)} \frac{\partial f}{\partial E} dE, \qquad (1)$$

where $E_i(\nu)$ are the bottoms of the magnetic field dependent subbands. Figure 2(a) shows the simulated MC for a 14 nm semiconducting CNT at 150 K and for various energies, ranging from the CNP to the second subband. The zero-field energy dependent conductance is also plotted in the inset, at 0 K (dotted line) and 150 K (solid line).

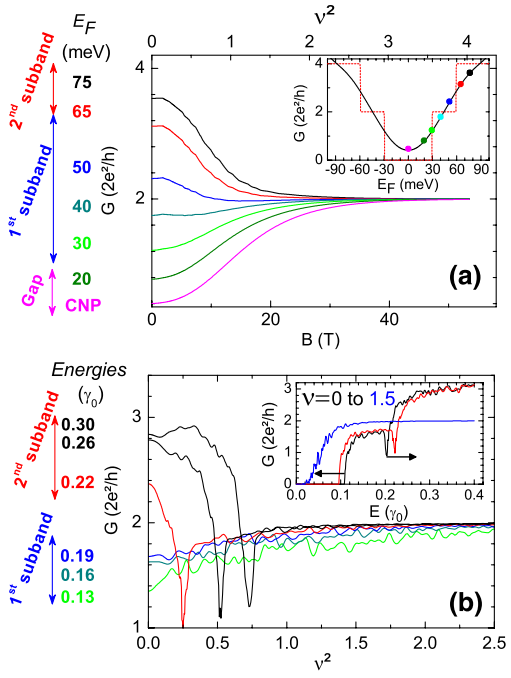

FIG. 2 (color online). (a) Simulated $G(B)$ using Eq. (1) in the ballistic regime for a 14 nm semiconducting CNT and different Fermi level locations. Inset: Zero-field conductance $G(E_F)$ at 0 K (dashed line) and 150 K (solid line), color dots indicate the chosen energies for $G(B)$. (b) $G(B)$ of a weakly disordered (17,0) tube for E_F in the first and second subbands using Eq. (2). Inset: $G(E_F)$ for $\nu = 0$ and 1.5. Note the $2G_0$ transmission for the Landau state in high field despite the presence of disorder (dot line).

A very good agreement with the experimental data is obtained for a similar energy window. While the increase of the conductance in the vicinity of the CNP is attributed to the onset of the first Landau state, i.e., the closing of the gap, the decrease of the conductance at higher energies corresponds to the depletion of the second subband. In the high field regime, the conductances merge to a common value as a result from the limited occupancy of the single Landau level, whatever the gate voltage value. Note that the experimental conductance value of $0.7G_0$ instead of the expected $2G_0$ may be explained by a nonperfect transmission at the contacts [9].

Magnetotransport properties beyond the ballistic regime are further explored by introducing a disorder potential $W = 0.3\gamma_0$ which allows us to quantitatively reproduce the experimental zero-field conductance (assuming an experimental transmission coefficient of 0.5 per channel at each contact). The low-bias, zero-temperature magnetoconductance is then expressed as

$$\langle G(E_F, \nu)\rangle = \frac{2e^2}{h}\langle T(E_f, \nu)\rangle, \qquad (2)$$

where the transmission factor is computed numerically by using standard iterative N order decimation techniques [15] and averaged over few tens of random configurations. Figure 2(b) shows the computed magnetoconductance for a (17,0) nanotube at three different energies, in the first and the second subband [16]. The strong conductance decay in the second subband, followed by a sharp minimum, describes the loss of two degenerate channels and the enhancement of the scattering when the vHs coincides with E_F. The simulation is clearly seen to reproduce the main experimental features except the vHs magnetofingerprint and related backscattering enhancement at moderate field. Experimental evidence of the crossing of vHs would certainly have required lower measurement temperature. The computed conductance versus energy for ν equal 0 and 1.5 are given in the inset of Fig. 2(b). Interestingly, despite the presence of some disorder, the high field conductance on the first Landau state converges to the ideal $2G_0$ value, suggesting a full suppression of backscattering. This strongly supports the formation of magnetic field induced delocalized states, which are likely to be originating from nondissipative left and right-moving snakelike currents at the opposite flanks of the nanotube.

For completeness, the Landau regime experienced by a semiconducting CNT is now compared to the Landau states that develop on a metallic CNT. The inset of Fig. 3(a) shows the Aharonov-Bohm quantum flux modulations of the conductance for selected back-gate voltages performed at 100 K on a MWCNT ($L_t \approx 180$ nm) and a magnetic field applied parallel to the tube axis. Three periods are identified, corresponding to a metallic external shell of 17.3 ± 0.5 nm diameter in agreement with the 18 nm estimated by AFM. We infer a CNP and the two first vHs in the n-doped state located at V_g equal to 4 ± 0.5 V (0 meV), 7 ± 0.5 V (70 meV), and 22 ± 2 V (140 meV—not shown here), respectively [9]. Figure 3(a) shows the transverse MC for various electrostatic doping varying from the CNP to the first diffusive band and Fig. 3(c) corresponds to selected curves in the doped state at low field (below 20 T). The low field data at 100 K within the first diffusive band unveil an initial decrease of the conductance followed by a local minimum (marked by an arrow) which is displaced to higher magnetic fields when E_F is upshifted. As for the semiconducting CNT, the decrease of the conductance is assigned to the upshift

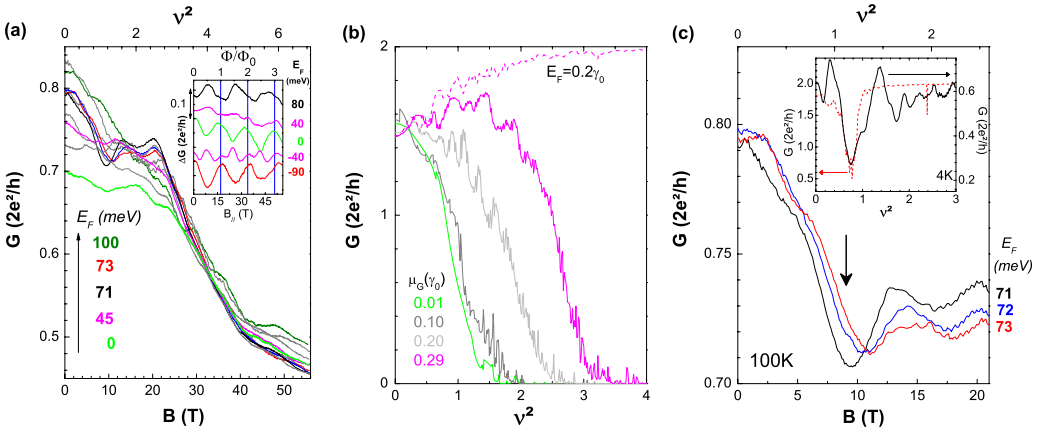

FIG. 3 (color online). (a) $G(B)$ measured at 100 K on a 17 nm MWCNT for various energies (from 0 to 100 meV) associated to different V_g (from 0 to 20 V). The metallic character of the outer shell together with the estimated Fermi energies are deduced from the Aharonov-Bohm MC obtained on the same MWCNT. Selected MC curves in parallel magnetic field are plotted in the inset [9]. (b) Computed MC including the field dependence of E_F in the metallic band for various μ_g. The calculated MC at a fixed Fermi energy ($E_F = 0.2\gamma_0$) is shown by the dotted line. (c) Low magnetic field experimental MC curves extracted from Fig. 3(a) for selected energies in the first diffusive band at 100 K. Inset: direct comparison of the experimental MC at 4 K for $E_F = 72$ meV (solid curve) with the calculated one for a (10,10) weakly disordered tube (dotted curve) for a similar energy, $E_F = 0.35\gamma_0$, in the first diffusive band.

of the first subband above E_F. From the locations of the minima for different doping levels, between 70 and 80 meV, we infer a $\partial E/\partial B$ variation of the order of 3 ± 0.5 meV/T, in agreement with the predicted $E_i(\nu)$ shifts for a similar range of magnetic field [7]. At 4 K [inset Fig. 3(c)], by reducing the thermal energy, the low field MC at $E_F = 72 \pm 2$ meV, slightly above the first vHs, develops a deep minimum superimposed on Fabry-Perot conductance modulations, already observed on similar devices [17].

A (10,10) metallic nanotube with a disorder strength of $W = 0.5\gamma_0$ is chosen for the simulation of a quasiballistic regime ($L_t \sim l_e$, l_e being the elastic mean free path evaluated from [18] at the CNP). The results are shown in Fig. 3(b). The sharp minimum of the calculated MC qualitatively reproduces the experiment for a similar doping ($E_F = 0.35\gamma_0$, just above the first vHs). Despite the weak disorder, a drastic increase of the backscattering occurs when the vHs is lined up with E_F.

The MC is now analyzed in the entire magnetic field range [Fig. 3(a)]. Remarkably, all the curves undergo a significant conductance decay for $B \geq 35$ T and converge toward a common quantum regime, irrespective of the electrostatic doping. In the vicinity of the first metallic bands, the conductance is initially weakly magnetic field dependent before experiencing a large decrease above $\nu \approx 1.7$. We interpret this phenomenon as the first experimental evidence of the reintroduction of the backscattering in the metallic band due to their magnetic field induced flattening and DOS increase, confirming a long standing prediction by Ando and co-workers [19].

To explain the clustering of the conductance curves in high field, one notices that the experiment is performed at a fixed back-gate voltage, so at a constant charge density. This constraint is translated into the physical assumption of complete balance between the electrostatic and the electronic charges: $q_{\mathrm{el}}(\mu_T, \mu_g) = q_{\mathrm{CNT}}(\mu_T, \nu)$ where the electrostatic charge $q_{\mathrm{el}}(\mu_T, \mu_g) = \kappa(\mu_T - \mu_g)$ is a function of the unknown Fermi energy $\mu_T(\mu_g, \nu)$ and of the gate voltage μ_g, and the electronic charge $q_{\mathrm{CNT}} = \int_0^{-\mu_T} dE\rho(E, \nu)$ is a functional of the magnetic field dependent DOS $\rho(E, \nu)$. The only input parameter is the capacitance per unit length κ, estimated from the experimental setup to $\kappa = 0.8$ [13].

A drastic magnetic field induced shift of the Fermi energy towards the CNP is observed once ν becomes larger than unity, even in the highly doped state [13]. This so-called pinning of E_F toward the CNP goes with the exponential enhancement of the DOS at zero-energy. The unknown Fermi energy of Eq. (2) is now replaced by the computed $\mu_T(\mu_g, \nu)$ in the conductance calculation of the (10,10) CNT [Fig. 3(b)]. At the CNP (green curve), when ν is increased, a Landau energy band develops in the DOS, resulting in the reintroduction of the backscattering and the large negative MC. At higher gate, the conductance also experiences a large decrease due to the magnetic field induced Fermi energy shift toward the CNP, consistent with the experiment. However, if one neglects the constant charge condition, the MC curve at a fixed Fermi energy exhibits the opposite behavior in high field and saturates to the ideal $2G_0$ value (dotted line). In conclusion, our measurements have evidenced the emergence of Landau levels in both semiconducting and metallic outer shells of MWCNTs, each case manifesting a characteristic evolution of the magnetoconductance.

Sample preparations were achieved at LAAS. Part of this work has been supported by EuroMagNET, EU Contract No. 228043. B. R. acknowledges A. Magrez for providing the MWCNTs. R. A. acknowledges funding from the Spanish MICINN under contract NAN2007-29366-E. Useful discussions with Pr. T. Ando and T. Nakanishi are acknowledged.

[1] J. C. Charlier, X. Blase, and S. Roche, Rev. Mod. Phys. **79**, 677 (2007); A. H. Castro Neto *et al.*, Rev. Mod. Phys. **81**, 109 (2009); A. Cresti *et al.*, Nano Res. **1**, 361 (2008).
[2] D. Mann *et al.*, Nano Lett. **3**, 1541 (2003).
[3] S. V. Morosov *et al.*, Phys. Rev. Lett. **100**, 016602 (2008).
[4] K. S. Novoselov *et al.*, Nature (London) **438**, 197 (2005).
[5] A. Bachtold *et al.*, Nature (London) **397**, 673 (1999); C. Coskun *et al.*, Science **304**, 1132 (2004).
[6] H. Ajiki and T. Ando, J. Phys. Soc. Jpn. **62**, 1255 (1993).
[7] H.-W. Lee and D. S. Novikov, Phys. Rev. B **68**, 155402 (2003); N. Nemec and G. Cuniberti, Phys. Rev. B **74**, 165411 (2006); E. Perfetto *et al.*, Phys. Rev. B **76**, 125430 (2007).
[8] J.-M. Bonard *et al.*, Adv. Mater. **9**, 827 (1997).
[9] S. Nanot *et al.*, C.R. Physique **10**, 268 (2009).
[10] The calculation is performed for a (179,0) CNT of 14 nm diameter. Choosing other indices for semiconducting CNT around 14 nm weakly impacts the locations of the vHs in the Dirac cone.
[11] R. Peierls, Z. Phys. **80**, 763 (1933).
[12] R. Avriller *et al.*, Mod. Phys. Lett. B **21**, 1955 (2007).
[13] See EPAPS Document No. E-PRLTAO-104-029001 for a detailed description of the calculation. For more information on EPAPS, see http://www.aip.org/pubservs/epaps.html.
[14] M. Büttiker, Y. Imry, R. Landauer, and S. Pinhas, Phys. Rev. B **31**, 6207 (1985).
[15] F. Triozon, Ph. Lambin, and S. Roche, Nanotechnology **16**, 230 (2005).
[16] Simulations of $G(B)$ are performed on smaller diameter tubes due to computational limitations. However, owing to conductance scaling properties [12], experimental and simulated data well agree for a given range of model parameters.
[17] B. Raquet *et al.*, Phys. Rev. Lett. **101**, 046803 (2008).
[18] C. T. White and T. N. Todorov, Nature (London) **393**, 240 (1998).
[19] T. Seri and T. Ando, J. Phys. Soc. Jpn. **66**, 169 (1997); T. Ando and T. Nakanishi, J. Phys. Soc. Jpn. **67**, 1704 (1998).